Nghiên cứu tổng hợp vật liệu nano Ni/NiO để nâng cao hiệu quả xúc tác quang phân hủy hỗn hợp chất màu methylene blue và rhodamine B

TÓM TẮT

Nghiên cứu đã tổng hợp thành công vật liệu nano Ni/NiO bằng phương pháp đốt cháy gel sử dụng imidazole và ứng dụng làm xúc tác quang phân hủy methylene blue (MB) và rhodamine B (RhB) dưới tác dụng của ánh sáng mặt trời. Vật liệu được đặc trưng bằng phương pháp nhiễu xạ tia X, hiển vi điện tử quét và phổ tán xạ năng lượng tia X. Kết quả xác nhận sự tồn tại đồng thời của các hạt nano NiO và Ni với kích thước tinh thể từ 9 đến 47 nm. Ảnh hưởng của điều kiện tổng hợp, bao gồm tỉ lệ mol imidazole/nickel, nhiệt độ và thời gian nung, đến hoạt tính quang xúc tác đã được khảo sát. Kết quả thực nghiệm cho thấy mẫu Ni/NiO(1:1) được tổng hợp ở 350 °C trong 10 phút thể hiện hoạt tính quang xúc tác cao nhất, với hằng số tốc độ biểu kiến bậc nhất đạt 0,0161 phút^{-1} đối với MB và 0,00757 phút^{-1} đối với RhB. Hoạt tính quang xúc tác của Ni/NiO được tăng cường là do hiệu ứng hiệp đồng giữa NiO và Ni, trong đó Ni đóng vai trò là bẫy electron hiệu quả, thúc đẩy quá trình phân ly điện tích và ức chế sự tái tổ hợp electron–lỗ trống theo cơ chế VB-CB-Ni. Các thí nghiệm bắt gốc tự do cho thấy gốc hydroxyl đóng vai trò chủ đạo trong quá trình quang phân hủy cả hai chất màu, trong khi vai trò của lỗ trống quang sinh và gốc superoxide là không đáng kể. Ngoài ra, vật liệu Ni/NiO thể hiện khả năng tái sử dụng tốt, với sự suy giảm hoạt tính quang xúc tác không đáng kể sau ba chu trình sử dụng liên tiếp.

Từ khóa: *Imidazole, vật liệu nano Ni/NiO, xúc tác quang, methylene blue, rhodamine B, ánh sáng mặt trời.*

Controlled synthesis of Ni/NiO nanocomposites for enhanced photocatalytic degradation of Methylene Blue and Rhodamine B

ABSTRACT

In the present paper, Ni/NiO nanocomposite photocatalyst was successfully synthesized through a facile one-step solution combustion method using nickel nitrate as the metal precursor and imidazole reductant as the reducing agent. This material was then applied for the solar-light-driven degradation of methylene blue (MB) and rhodamine B (RhB). The obtained material was characterized by X-ray diffraction, scanning electron microscopy and energy dispersive X-ray. The physicochemical characterization confirmed the presence of the nanoparticles NiO and Ni with crystalline size from 9 nm to 47 nm. The effect of synthesis conditions, including the molar ratio of imidazole/nickel, calcination temperature and time, on the photocatalytic performance was systematically investigated. The experimental results revealed that Ni/NiO(1:1) catalyst prepared at 350 °C for 10 min exhibited the highest photocatalytic activity, with apparent first-order rate constants of 0.0161 min^{-1} for MB and 0.00757 min^{-1} for RhB under natural sunlight. The enhanced photocatalytic performance is attributed to the synergistic interaction between NiO and metallic Ni, in which Ni acts as an effective electron sink, facilitating charge separation and suppressing electron–hole recombination through the VB-CB-Ni mechanism. Radical trapping experiments demonstrated that hydroxyl radicals play a dominant role in the photocatalytic degradation of both dyes, while photogenerated holes and superoxide radicals contribute negligibly. Furthermore, the Ni/NiO catalyst exhibited good recyclability, with only a slight decrease in photocatalytic activity after three successive cycles.

Keywords: *Imidazole, Ni/NiO nanoparticles, photocatalyst, methylene blue, rhodamine B, natural sunlight.*

1. INTRODUCTION

In recent years, environmental pollution has become one of the most pressing issues globally. The rapid growth of industrial activities has been identified as a major contributor to the severe degradation of the global environment. Industrial effluents, particularly from textile processing, are notably rich in dye compounds, contributing significantly to water pollution. The discharge of effluents from textile industries into water bodies results in severe water pollution in many regions worldwide. Various physical, chemical, and biological approaches, as well as their combinations, have been employed for the treatment of dye-containing wastewater. Among these methods, photocatalytic degradation has been recognized as an effective and cost-efficient technique due to its simple design and operational feasibility.[1-3]

Photocatalytic semiconductor materials, such as TiO_2, ZnO, NiO, WO_3, and Fe_2O_3, have attracted considerable attention due to their strong oxidative power, chemical stability, low cost, and non-toxicity. Among metal-oxide semiconductors, NiO has been extensively studied owing to its distinctive photocatalytic and magnetic properties and has been employed as a photocatalyst for the degradation of various environmental pollutants.[4-9] Nevertheless, NiO materials exhibit inherent limitations arising from their wide band gap (3.2-4.2 eV), which restricts light absorption primarily to the UV region, and from the rapid recombination of photogenerated electron-hole pairs, resulting in diminished photocatalytic performance.[10-12] To address these limitations and enhance the photocatalytic performance, doping and combining NiO with other materials have been employed.[13-15] One effective strategy to enhance photocatalytic activity is the use of metal/metal oxide systems, which can exploit the synergistic interactions between the two components. It has been reported that Ni^0 sites act as electron traps during the photocatalytic process. This trapping of electrons delays their recombination with holes, which are also generated by light irradiation. By mitigating electron–hole recombination, Ni^0 significantly enhances the overall photocatalytic performance.[12,16] Numerous methods have been developed for the synthesis of Ni/NiO materials.[17-21] In particular, the combustion of organic nickel precursors represents a straightforward synthesis approach, which can produce highly active Ni/NiO materials.[22-26] It has been reported that synthesis'

conditions affect the morphology, particle size, Ni/NiO ratio, thereby affecting the applicability of the material.[27,28]

In the present paper, we report the synthesis of Ni/NiO nanomaterials via solution combustion route using a nickel–imidazole precursor and the systematic investigation of their photocatalytic activity toward the degradation of methylene blue and rhodamine B under natural sunlight. Furthermore, the effects of key synthesis parameters, including organic ligand content, calcination temperature, and calcination time, on the photocatalytic performance of the obtained materials were thoroughly examined.

2. EXPERIMENTAL

2.1. Chemicals

All chemicals utilized within this study were of analytical grade and were used as received without any further purification. All solutions were prepared with double-distilled water. The following reagents were used: $Ni(NO_3)_2.6H_2O$ (AR, 98.5%, Sigma Aldrich, America), imidazole (AR, 99%, Acros, America), ethanol (AR, 99%, Xilong, China), rhodamine B (AR, 95%, Sigma Aldrich, America), methylene blue (AR, 98.5%, Xilong, China), methanol (AR, 99.5%, Xilong, China), 1,4-benzoquinone (AR, 99%, Acros, America), amoni oxalate (AR, 99%, Xilong, China).

2.2. Synthesis of the Ni/NiO nanocomposites

0.002 mol of $Ni(NO_3)_2$ was dissolved into 10 mL of double-distilled water under magnetic stirring, followed by the addition n mol of imidazole (n = 0.002-0.012 mol). The mixture was further stirred for another 15 minutes. The resulting solution was placed in a high heat-insulated porcelain crucible and evaporated on a hot plate. The resulting product was then heated at temperatures T ^oC (T = 300-500 ^oC) for t minute (t = 5-40 min). Materials synthesized from nickel nitrate and imidazole at molar ratios of 1:1; 1:2; 1:4; 1:6 are denoted as Ni/NiO(1:1), Ni/NiO(1:2), Ni/NiO(1:4), Ni/NiO(1:6) respectively. For comparision, pristine NiO sample was synthesized in a same manner with the use of solely $Ni(NO_3)_2$.

2.3. Characterizations

The obtained sample was characterized by using various chemical and physical techniques. The X-ray diffraction (XRD) patterns were recorded on a Bruker D8-Advance X-ray powder diffractometer using Cu K_α radiation (λ = 1.5406 Å) with scattering angles (2θ) of 30-80°. The crystalline size is determined according to the Scherrer formula:[29]

$$D = \frac{K\lambda}{\beta \cos\theta} \quad (1)$$

where D is the average crystalline size (nm), K is Scherrer constant (K = 0.94); λ is a wavelength in Å (λ = 1.5418 Å), β is the Full width at half maximum (radian) and θ is diffraction angle (degree).

The major diffraction peaks at 2θ, 37.2^o and 51.7^o, which can be indexed as (111) plane for NiO and (200) plane for Ni were used to calculate the crystal size.

The composition of the solid products was identified by the Rietveld method using the TOPAS program (TOPAS-Total Pattern Analysis System, Version 4.2, Bruker AXS).

Scanning electron microscopy (SEM) and mapping energy dispersive X-ray spectroscopy (EDX) were performed on an SEM-JEOL-JSM 5410 LV (JEOL JSM-IT200, Japan) with an acceleration voltage of 10 kV at a magnification level of 10 K.

2.4. Adsorption study

An amount of 30 mg of the synthesized material was added to a beaker containing 100 mL of a mixed solution of methylene blue (MB, 10 ppm) and rhodamine B (RhB, 2 ppm). The mixture was kept in the dark to prevent any photodegradation and was continuously stirred using a magnetic stirrer to ensure thorough mixing. At 30-min intervals, approximately 3 mL of the solution was withdrawn and the concentrations of the remaining dyes were determined using a UV-Vis spectrophotometer (Lambda 365, Perkin Elmer, USA). The adsorption process was continued until the dye concentrations reached equilibrium, indicated by negligible changes over time.

Adsorption efficiency (H%) is determined by the formula:

$$H(\%) = \frac{C_0^{'} - C}{C_0^{'}} \times 100\% \quad (2)$$

where $C^{'}_0$ is the initial concentration of the dye; C is the remaining concentration of the dye after reaching adsorption equilibrium.

2.5. Photocatalytic degradation experiments

After reaching adsorption equilibrium, the mixed dye solution was exposed to sunlight

between 10 h and 13 h on sunny days, with an average ambient temperature of 36-39 °C. At 30-min intervals, approximately 3 mL of the solution was withdrawn and analyzed using a UV-Vis spectrophotometer to determine the remaining dye concentration. The apparent rate constant (k) of the photocatalytic degradation was determined using the Langmuir–Hinshelwood model by plotting $\ln(C_0/C)$ as a function of time (t), where C_0 and C represent the dye concentrations before and after irradiation, respectively. The slope of the linear regression was used to calculate k.

To identify the active species responsible for the photocatalytic degradation of the dyes, radical scavengers were employed to selectively quench specific reactive species: methanol (Me) for hydroxyl radicals ($^{\cdot}OH$), benzoquinone (BQ) for superoxide radicals ($O_2^{(\bullet-)}$), and ammonium oxalate (AO) for photogenerated holes (h^+). For each experiment, 20 mL of either deionized water, absolute Me, 5 mM BQ, or 5 mM AO was added to 100 mL of a mixed dye solution containing 10 ppm MB and 2 ppm RhB with 0.3 g/L Ni/NiO catalyst, which had previously reached adsorption equilibrium. The photocatalytic experiments were then conducted under the same irradiation conditions.

The recovery and reusability of the Ni/NiO photocatalyst were evaluated using a mixed solution of MB and RhB. After 3 h of solar irradiation, the catalyst was recovered by decantation, thoroughly washed several times with deionized water and 96° ethanol, and then dried at 80 °C for 30 min. The recovered Ni/NiO material was subsequently reused in the next photocatalytic cycle under identical experimental conditions.

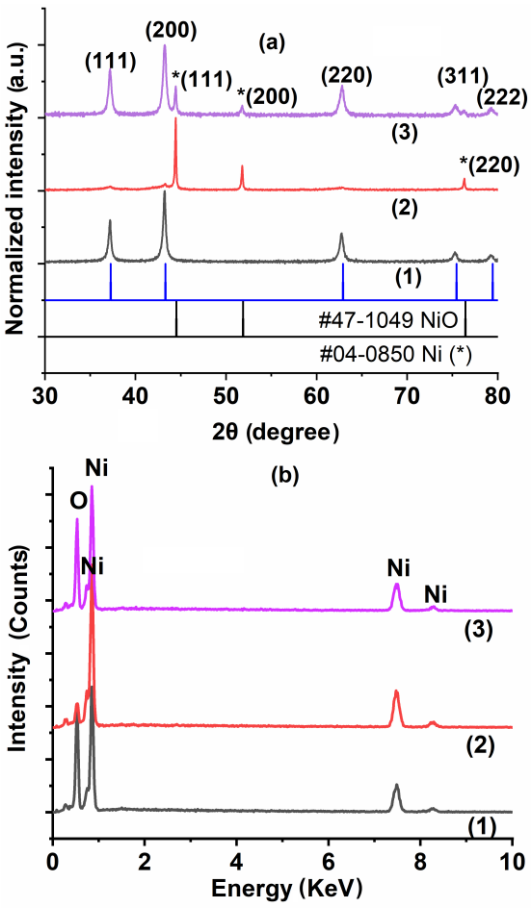

3. RESULTS AND DISCUSSION

3.1. The characterization of materials

Figure 1a shows the XRD patterns of materials synthesized from nickel nitrate and imidazole at various molar ratios.

Figure 1. XRD patterns (a) and EDX (b) of the samples: (1) – NiO; (2) – Ni/NiO(1:1); (3) – Ni/NiO(1:6)

The XRD pattern of sample synthesized from nickel nitrate exhibits the characteristic peaks at 37.2, 43.2, 62.8, 75.6, and 79.4° indexed to the (111), (200), (220), (311), and (222) planes of NiO according to JCPDS 47-1049.[30] The XRD patterns of samples synthesized from the combustion of nickel – imidazole mixture, in addition to the characteristic peaks for NiO, exhibit the characteristic peaks at 44.5; 51.8 and 76.3° which are indexed to the (111), (200), (220) planes of Ni according to JCPDS 04-0850.[28] Interestingly, with increasing imidazole/nickel ratios, the intensity of characteristic peaks of Ni decreases, whereas that of NiO increases.

The phase composition and crystalline size of Ni/NiO samples were calculated from XRD data. The results indicate that in the Ni/NiO (1:1) sample, the metallic nickel phase accounts for 91%. Increasing the molar ratio of imidazole to nickel leads to a gradual decrease in the Ni content to only 18% in the Ni/NiO(1:6) sample. The nickel-imidazole molar ratio not only affects the phase composition but also the crystalline size of the resulting material. As the molar ratio of imidazole to nickel increases, the crystalline size of metallic Ni decreases, while the crystalline size of NiO gradually increases (Table 1).

Table 1. The characterization of materials based on XRD and EDX analysis

Characterization		Sample		
		NiO	Ni/NiO(1:1)	Ni/NiO(1:6)
Phase composition (%)	Ni	0	81	18
	NiO	100	9	82

Crystalline size (nm)	Ni		47	25
	NiO	20	9	17
Elemental composition (Atomic (%))	Ni	41.71	81.52	47.03
	O	58.29	18.48	52.97

The formation of metallic nickel can be attributed to the presence of nitrogen in imidazole. One of the thermolysis products of N-containing organic compounds is ammonia, which can participate in the reduction of nickel oxide.[31] However, when the molar ratio of imidazole to nickel nitrate is large, corresponding to an oxygen-deficient mixture, the combustion reaction predominantly consumes oxygen from the ambient atmosphere, leading to a vigorous reaction and consequently the formation of nickel oxide. In contrast, when the imidazole-to-nickel nitrate molar ratio is small, i.e oxygen-rich mixture, the combustion reaction occurs mildly forming NH_3, the combustion process proceeds more mildly and generates NH_3, which promotes the formation of metallic Ni with a larger crystallite size.[26,31]

The EDX spectrum shown in Fig. 1b further confirms the presence of nickel and oxygen in the synthesized Ni/NiO materials. The results indicate that the O/Ni atomic ratios in the NiO and Ni/NiO(1:6) samples are higher than the stoichiometric value of 1:1 (Table 1), suggesting preferential oxygen adsorption on the NiO surface.

The surface morphology of the materials is revealed from the SEM images (Fig. 2). The NiO sample synthesized from $Ni(NO_3)_2$ exhibits discrete and well-defined octahedral particles. In contrast, the Ni/NiO samples prepared from the nickel–imidazole precursor show pronounced particle agglomeration. Such agglomeration may facilitate interparticle contact and enhance charge transport within the material, thereby contributing to improved photocatalytic performance.

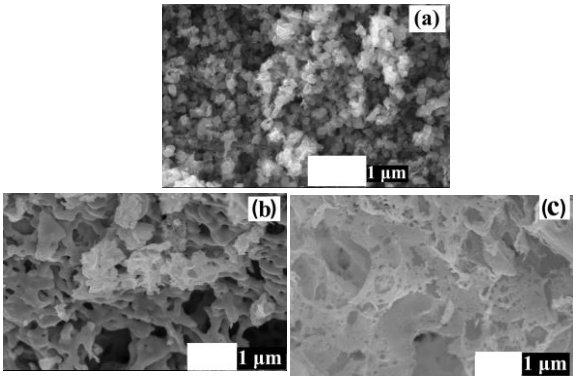

Figure 2. SEM images of the samples NiO (a); Ni/NiO(1:1) (b); Ni/NiO(1:6) (c)

3.2. Photocatalytic performance of Ni/NiO materials for dye degradation

The time-dependent UV–Vis absorption spectra of the mixed MB and RhB solution in the presence of Ni/NiO under solar light irradiation are presented in Fig. 3a. Two characteristic absorption maxima are observed in the visible region, located at 554 nm, corresponding to the π–π transition of RhB, and at 664 nm, attributed to the n–π* transition of MB (where n denotes the lone pair of electrons on the nitrogen atom of the C=N bond and the sulfur atom of the S=C bond).[32,33] With increasing irradiation time, the absorbance intensities of both dyes decrease progressively. After approximately 180 min of solar irradiation, the characteristic absorption peak of RhB decreases to about three-quarters of its initial height, whereas the absorption peak of MB almost completely disappears.

To evaluate the dye removal performance of Ni/NiO materials toward MB and RhB, a series of parallel experiments were conducted using a mixed dye solution containing 10 ppm MB and 2 ppm RhB under different reaction systems: (i) without catalyst, (ii) in the presence a NiO catalyst, and (iii) Ni/NiO catalysts.

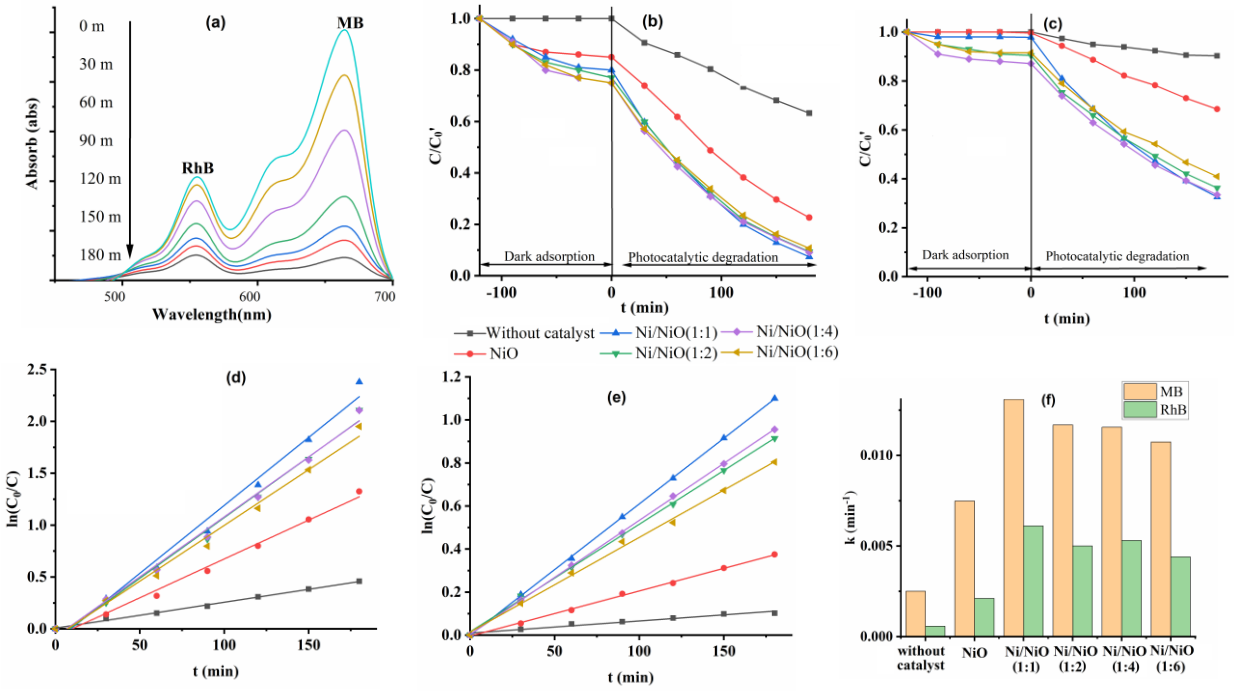

Figure 3. UV–Vis absorption spectra of the mixed MB and RhB solution under solar irradiation as a function of time; temporal evolution of MB (b) and RhB (c) concentrations; pseudo-first-order kinetic plots ln(C_0/C) versus irradiation time for MB (d) and RhB (e); dependence of the apparent rate constants for MB and RhB degradation on the catalyst material (f).

The temporal variations in the concentrations of MB and RhB for the different reaction systems are shown in Fig. 3b and Fig. 3c, respectively. The experimental results indicate that both MB and RhB are relatively stable under dark conditions. Upon solar light irradiation, both dyes undergo slow degradation over time. Among the two dyes, RhB exhibits higher stability than MB. After 180 min of solar irradiation, approximately 36% of MB is degraded, whereas only about 9% of RhB is decomposed. Upon the addition of NiO, approximately 15% of MB is removed in the dark due to adsorption. Under solar light irradiation, the concentrations of both MB and RhB decrease markedly with irradiation time. After 180 min of irradiation, the removal efficiencies reach approximately 77% for MB and 32% for RhB. When Ni/NiO material is used, the amount of dye removed via adsorption in the dark increases remarkedly, ranging from 20% to 25% for MB and from 2% to 12% for RhB, depending on Ni/NiO ratio in the material. After 180 min of solar light irradiation, the dye removal efficiency is also significantly enhanced, reaching approximately 89–93% for MB and 59–67% for RhB.

The plots of ln(C_0/C) versus irradiation time exhibit a linear relationship with a high coefficient of determination (R^2 = 0.99), as shown in Fig. 3d and Fig. 3e. This behavior is in good agreement with the Langmuir–Hinshelwood kinetic model, indicating that MB and RhB undergo photocatalytic degradation and that the degradation process follows pseudo-first-order reaction kinetics.[34] The photocatalytic degradation rate constants for MB and RhB were determined from the slopes of the corresponding linear plots. The calculated results show that the presence of NiO increases the photocatalytic degradation rate constants of MB and RhB by factors of 3.0 and 3.7, respectively. Meanwhile, the Ni/NiO material at the same catalyst loading enhances the rate constants by 5.2 times for MB and 10.7 times for RhB. With increasing imidazole-to-nickel molar ratio, the photocatalytic degradation rates of both MB and RhB slightly decrease. Among the investigated samples, Ni/NiO (1:1) exhibits the highest photocatalytic activity (Fig. 3f).

As is well known, during the photocatalytic process, reactive species play a crucial role in dye degradation, including photogenerated holes, superoxide radicals, and hydroxyl radicals. In practice, methanol is commonly used as a scavenger for $^{\cdot}OH$ radicals, benzoquinone acts as an effective scavenger for $O_2^{(\cdot-)}$ radicals, while ammonium oxalate is employed as a h^+ scavenger.[35] The effects of different scavengers on the photocatalytic degradation rates of MB and RhB over the Ni/NiO catalyst are presented in Fig. 4.

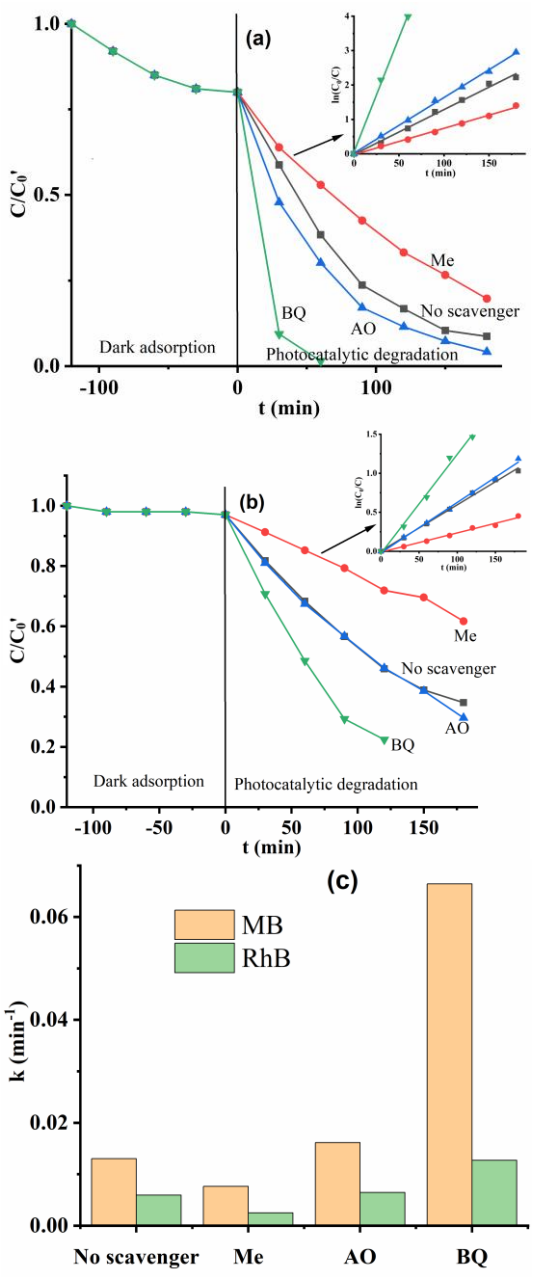

Figure 4. Effects of Me, AO, and BQ scavengers on the kinetics of photocatalytic degradation of MB (a, c) and RhB (b, c) over the Ni/NiO catalyst.

The experimental results indicate that the photocatalytic activity of Ni/NiO toward dye degradation gradually decreases upon the addition of methanol. In contrast, when ammonium oxalate is introduced into the reaction system, the photocatalytic degradation rate of MB slightly increases, while that of RhB remains almost unchanged. For both dyes, the addition of benzoquinone leads to a significant enhancement in the degradation rate. These observations suggest that hydroxyl radicals are the dominant oxidative species responsible for the photocatalytic degradation of MB and RhB on the Ni/NiO surface, whereas the contributions of photogenerated holes and superoxide radicals are relatively minor. The enhanced photocatalytic degradation observed upon the addition of $O_2^{(\bullet-)}$ and h^+ scavengers can be attributed to the suppression of electron–hole recombination. Specifically, the scavenging of $O_2^{(\bullet-)}$ and h^+ promotes the separation of photogenerated charge carriers and facilitates electron consumption, thereby increasing the availability of holes for $^{\bullet}OH$ generation, which accelerates dye degradation.[36,37]

In the absence of a catalyst, the degradation of MB and RhB under solar irradiation mainly proceeds via a direct photolysis process. Upon light irradiation, MB and RhB molecules absorb photons and become photoexcited, resulting in the promotion of an electron from the highest occupied molecular orbital (HOMO) to the lowest unoccupied molecular orbital (LUMO), leaving a corresponding hole in the HOMO level. The excited electrons in the LUMO can interact with dissolved oxygen molecules or water molecules to generate reactive oxygen species, particularly hydroxyl radicals, which then participate in the oxidative degradation of the dye molecules. However, due to the limited light absorption capacity of MB and RhB under solar irradiation and the low efficiency of photonic energy conversion, the amount of generated $^{\bullet}OH$ radicals in the non-catalytic system is relatively small. In addition, the excited states of the dye molecules have short lifetimes and are prone to non-radiative relaxation processes. As a result, the generation of reactive oxidative species is inefficient, leading to a relatively slow degradation rate of MB and RhB.

When NiO is introduced into the system, it acts as a semiconductor photocatalyst. Upon solar light irradiation, NiO absorbs photons with energy equal to or greater than its band gap, leading to the excitation of electrons from the valence band (VB) to the conduction band (CB) and the simultaneous generation of photogenerated holes (h^+) in the VB. The photoinduced holes in the valence band and electrons in the conduction band subsequently participate in surface redox reactions, leading to the formation of hydroxyl radicals, which play a dominant role in the degradation of MB and RhB molecules. In addition, the adsorption capability of NiO toward MB and RhB contributes to an increased apparent reaction rate by enriching the dye molecules in the vicinity of

the active sites, where photocatalytic reactions preferentially occur. This synergistic effect between light-induced charge carrier generation and dye adsorption effectively promotes the photocatalytic degradation efficiency.

In the Ni/NiO composite system, NiO acts as the primary semiconductor photocatalyst, while metallic Ni⁰ serves as an efficient electron sink, forming a metal–semiconductor heterojunction. Due to the favorable band alignment and the formation of a Schottky junction at the Ni/NiO interface, the photogenerated electrons in the CB of NiO are readily transferred to the metallic Ni⁰ phase. This electron migration is thermodynamically driven by the lower Fermi level of Ni⁰ and effectively suppresses the recombination of electron–hole pairs within NiO, consequently, higher photocatalytic degradation rates. However, as the imidazole-to-nickel molar ratio increases, the content of metallic Ni in the Ni/NiO composites decreases, leading to a gradual decline in photocatalytic activity. The reduced amount of metallic Ni weakens the electron-trapping effect and diminishes charge carrier separation efficiency, thereby accelerating electron–hole recombination. As a result, fewer reactive oxygen species are available for dye degradation, causing a decrease in the photocatalytic degradation rate constants of MB and RhB. The oxidation pathway of MB and RhB is illustrated schematically as follows:[6,16]

Photon excitation:

$$MB/RhB \xrightarrow{h\nu} MB/RhB^{*}(e^{-}_{LUMO} + h^{+}_{HOMO}) \quad (3)$$

$$NiO \xrightarrow{h\nu} NiO^{*}(e^{-}_{CB} + h^{+}_{VB}) \quad (4)$$

Formation of reactive oxygen species:

$$e^{-}_{LUMO} + O_2 \rightarrow O_2^{\bullet -} \quad (5)$$

$$e^{-}_{LUMO} + H_2O \rightarrow {}^{\bullet}OH + OH^{-} \quad (6)$$

$$e^{-}_{VB}(NiO) \rightarrow e^{-}(Ni) \quad (7)$$

$$e^{-}(Ni) + O_2 \rightarrow O_2^{\bullet -} \quad (8)$$

$$h^{+}_{VB}(NiO) + H_2O \rightarrow H^{+} + {}^{\bullet}OH \quad (9)$$

$$O_2^{\bullet -} \xrightarrow{H^{+}} HO_2^{\bullet} \xrightarrow{-O_2} H_2O_2 \rightarrow 2\,{}^{\bullet}OH \quad (10)$$

Oxidative degradation of dyes:

$$MB/RhB + {}^{\bullet}OH \rightarrow products \quad (11)$$

Charge recombination:

$$e^{-}_{LUMO} + h^{+}_{HOMO} \rightarrow MB/RhB \quad (12)$$

3.3. Effect of synthesis conditions Ni/NiO

The synthesis conditions, particularly calcination temperature and calcination time, have a pronounced influence on the photocatalytic activity of the Ni/NiO materials (Figure 5).

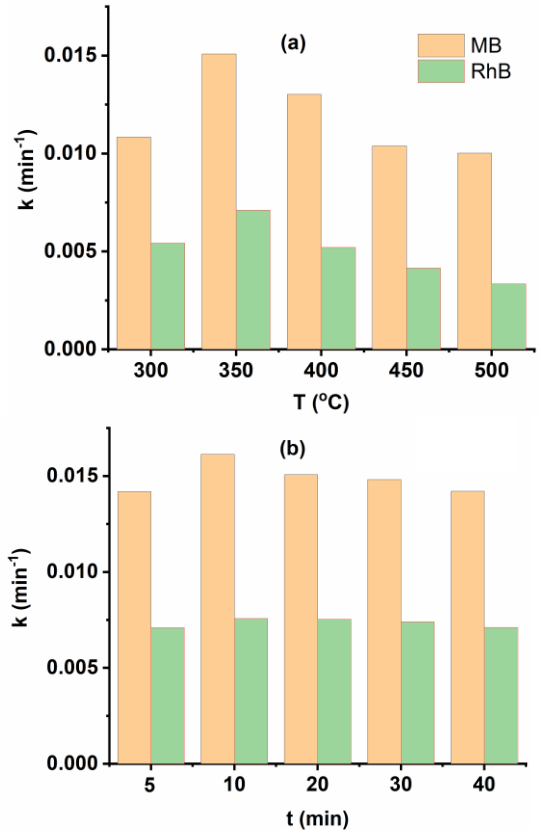

Figure 5. Photocatalytic degradation rate constants of MB and RhB in the presence of the Ni/NiO(1:1) catalyst synthesized at different calcination temperatures for 20 min (a) and different calcination times at 350 °C (b).

Experimental results indicate that when the calcination temperature increases from 300 to 500 °C, the photocatalytic degradation activity of the corresponding Ni/NiO catalyst initially increases and then gradually decreases. The highest photocatalytic degradation rate constants for both MB and RhB are achieved when using the Ni/NiO catalyst synthesized at 350 °C. The dependence of photocatalytic activity on calcination temperature can be explained by the partial re-oxidation of metallic Ni formed to NiO during the synthesis under the action of atmospheric oxygen as the temperature increases. This process increases the number of photoactive catalytic sites and promotes interfacial charge transfer. However, at excessively high calcination temperatures, most

of the metallic nickel is oxidized to NiO, which eliminates the synergistic effect, leading to a decrease in photocatalytic degradation efficiency.

With respect to calcination time, increasing the duration from 5 to 40 min results in only slight changes in the photocatalytic activity of the Ni/NiO catalyst. The maximum photocatalytic degradation rates of MB and RhB are obtained for the catalyst calcined at 350 °C for 10 min. This behavior can be attributed to the fact that at short calcination times (e.g., 5 min), only a small fraction of NiO is reduced to metallic Ni, and thus weak electron trapping capability, resulting in poor photocatalytic performance. As the calcination time increases, a favorable amount of metallic Ni is formed, enhancing charge separation and photocatalytic activity. However, prolonged calcination leads to re-oxidation of the surface Ni layer to NiO, thereby reducing the photocatalytic efficiency.

Moreover, excessive calcination temperature and time promote particle growth and agglomeration, reducing the specific surface area and limiting the accessibility of active interfacial sites, further impairing the efficiency of charge separation and photocatalytic degradation.

3.4. Catalyst recovery and reusability

The experimental results show that the photocatalytic activity of Ni/NiO for the degradation of MB and RhB slightly decreases after three reuse cycles. After the third reuse, the rate constant for MB decreased by approximately 25%, while that for RhB decreased by about 17%. These findings indicate that the Ni/NiO catalyst can be effectively recovered and reused, although its photocatalytic activity gradually declines with successive cycles.

Compared with other reported Ni-based catalysts, the Ni/NiO material synthesized in this work has better catalytic performance (Table 2).

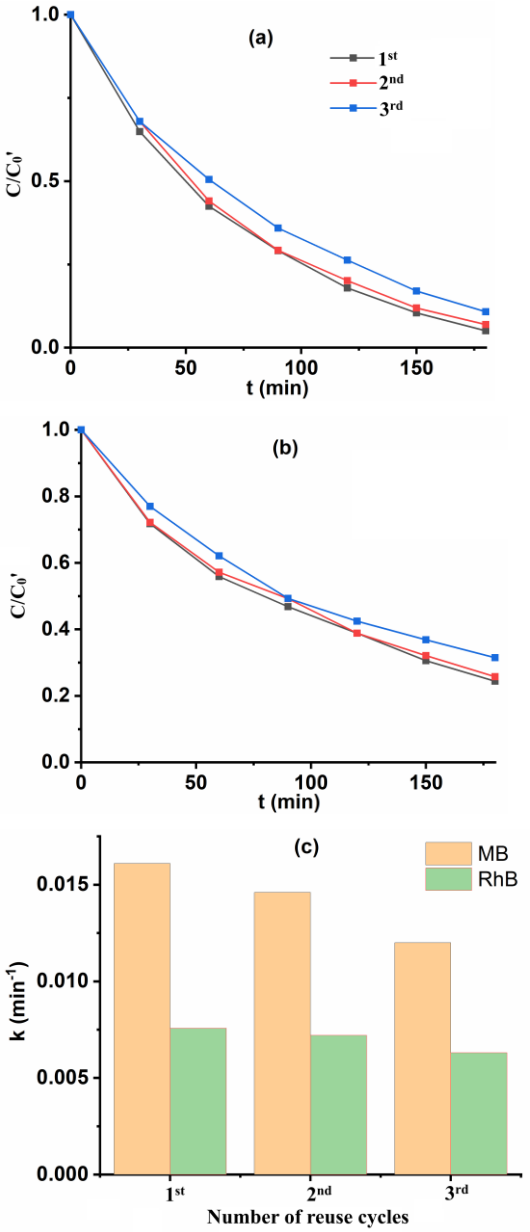

Figure 6. Temporal evolution of MB (a) and RhB (b) concentrations and the photocatalytic degradation rate constants of the dyes (c) after three reuse cycles of the Ni/NiO catalyst.

Table 2. Evaluation of photocatalytic degradation of MB and RhB dye under solar light with reported literature data

Catalyst	k (min^{-1})		Reference
	MB	RhB	
Ni/NiO	0.0161	0.00757	This work
Pt-Ni/NiO	0.01779		[12]
NiO	0.0082		[38]
ZnO/NiO	0.0058		[39]
CdO		0.0036	[40]
NiO-CaO		0.00459	[41]

3. CONCLUSION

In summary, a Ni/NiO photocatalyst was successfully synthesized via a simple combustion approach using a nickel–imidazole precursor demonstrating effective photocatalytic degradation of methylene blue and rhodamine B under natural sunlight. The photocatalytic activity was strongly influenced by the synthesis conditions, with the Ni/NiO (1:1) sample prepared at 350 °C for 10 min exhibiting the highest performance. The enhanced activity is mainly attributed to the synergistic interaction between NiO and metallic Ni, in which Ni^0 functions as an efficient electron sink, facilitating charge separation and suppressing electron–hole recombination through the VB-CB-Ni^0 pathway. In addition, the catalyst showed acceptable stability and reusability over three consecutive cycles. These findings highlight the potential of Ni/NiO as a cost-effective and recyclable photocatalyst for solar-driven dye degradation in wastewater treatment.

Acknowledgments

REFERENCES

1. M. Kumar, V. P. Singh, S. B. Bhat, R. Kumar. Environmental risks of textile dyes and photocatalytic materials for sustainable treatment: current status and future directions, *Discover Environment*, **2025**, *3*(132), 1-36.
2. H. Kumari, Sonia, Suman, R. Ranga, S. Chahal, S. Devi, S. Sharma, S. Kumar, P. Kumar, S. Kumar, A. Kumar, P. Rajesh. A review on photocatalysis used for wastewater treatment: dye degradation, *Water air soil pollut*, **2023**, *234*(349), 1-46.
3. V. T. Duyen, D. V. Tac. The synthesis Ag/Fe_3O_4 nanoparticles using guava leaf extract (psidium guajava l.) and its application for catalytic reduction of methylene blue and rhodamine B, *Chemchemtech*, **2025**, *68*(4), 41-48, 2025.
4. G. Jayakumar, A. A. Irudayaraj, A. D. Raj. Photocatalytic degradation of methylene blue by nickel oxide nanoparticles, *Materials Today: Proceedings*, **2016**, *4*(2017), 11690–11695.
5. Z. Sabouria, A. Akbaria, H. A. Hosseinia, M. Darroudi. Facile green synthesis of NiO nanoparticles and investigation of dye degradation and cytotoxicity effects, *Journal of molecular structure*, **2018**, *1173*, 931-936.
6. S. D. Khairnar, V. S. Shrivastava. Facile synthesis of nickel oxide nanoparticles for the degradation of Methylene blue and Rhodamine B dye: a comparative study, *Journal of Taibah University for Science*, **2019**, *13*(1), 1108-1118.
7. D. Blizak, S. Remli, S. Blizak, O. Bouchenak, K. Yahiaoui. NiO thin films for environmental photocatalytic applications: a review, *Algerian Journal of Environmental Science and Technology*, **2021**, *7*(2), 1950-1957.
8. F. Torki, H. Faghihian. Photocatalytic activity of NiS, NiO and coupled NiS–NiO for degradation of pharmaceutical pollutant cephalexin under visible light, *RSC Advances*, **2017**, *7*, 54651.
9. A. K. H. Bashira, L. Razanamahandrya, A. C. Nwanya, K. Kaviyarasua, W. Sabana, H. E. A. Mohameda, S. C. Nwtamped, F. I. Ezema, M. Maaza. Biosynthesis of NiO nanoparticles for photodegradation of free cyanide solutions under ultraviolet light, *Journal of Physics and Chemistry of Solids*, **2019**, *134*, 133-140.
10. M. Bonomo. Synthesis and characterization of NiO nanostructures: a review, *J. Nanopart Res*, **2018**, *20*(222), 1-26.
11. M. Taeño, D. Maestre, A. Cremades. An approach to emerging optical and optoelectronic applications based on NiO micro and nanostructures, *Nanophotonics*, **2021**, *10*(7), 1785-1799.
12. A. E. Noua, D. Kaya, G. Sigircik, T. Tuken, F. Karadag, A. Ekicibil. Methylene blue degradation with Pt-enhanced Ni/NiO nanocomposites: Adsorption, photocatalytic and magnetic insights, *Inorganic Chemistry Communications*, **2025**, *177*, 114388.
13. J. Al-Boukhari, A. Khalaf, R. S. Hassan, R. Awad. Structural, optical and magnetic properties of pure and rare earth doped NiO nanoparticles, *Applied Physics A*, **2020**, *126*(323), 1-13.
14. A. S. Bhatt, R. Ranjitha, M. S. Santosh, C. R. Ravikumar, S. C. Prashantha. Optical and electrochemical applications of Li-doped NiO nanostructures synthesized via facile microwave technique, *Materials*, **2020**, *13*, 2961.
15. A. A. A. Ahmed, E. A. A. Alahsab, A. M. Abdulwahab. The influence of Zn and Mg doping on the structural and optical properties of NiO nano-structures for optoelectronic applications, *Results in Physics*, **2021**, *22*, 103938.
16. S. K. Mohamed, A. M. Elhgrasi, O. I. Ali. Facile synthesis of mesoporous nano Ni/NiO and its synergistic role as super adsorbent and photocatalyst under sunlight irradiation, *Environmental Science and Pollution Research*, **2022**, 29, 64792-64806.

17. N. Srinivasa, J. P. Hughes, P. S. Adarakatti, C. Manjunatha, S. J. Rowley-Neale, S. Ashoka, C. E. Banks. Facile synthesis of Ni/NiO nanocomposites: the effect of Ni content in NiO upon the oxygen evolution reaction within alkaline media, *RSC Advances*, **2021**, *11*, 14654–14664

18. S. Adhikari, G. Madras. Role of Ni in hetero-architectured NiO/Ni composites for enhanced catalytic performance, *Phys Chem Chem Phys*, **2017**, *19*, 13895-13908.

19. S. Wang, P. Xu, J. Tian, Z. Liu, L. Feng. Phase structure tuning of graphene supported Ni-NiO nanoparticles for enhanced urea oxidation performance, *Electrochimica Acta*, **2021**, *370*, 137755.

20. Shivangi, S. Bhardwaj, T. Sarkar. Core–shell type magnetic Ni/NiO nanoparticles as recyclable adsorbent for Pb (II) and Cd (II) ions: One-pot synthesis, adsorption performance, and mechanism, *Journal of the Taiwan Institute of Chemical Engineers*, **2020**, *113*, 223-230.

21. J. Zhao, J. Zha, H. Lu, C. Yang, K. Yan, X. Meng. Cauliflower-like Ni/NiO and NiO architectures transformed from nickel alkoxide and their excellent removal of Congo red and Cr (VI) ions from water, *The royal society of chemistry*, **2016**, *6*, 103585–103593.

22. O. Thoda, G. Xanthopoulou, V. Prokof'ev, S. Roslyakov, G. Vekinis, A. Chroneos. Influence of Preheating Temperature on Solution Combustion Synthesis of Ni–NiO Nanocomposites: Mathematical Model and Experiment, *Int. J Self-Propag. High-Temp. Synth.*, **2018**, *27*, 207-215.

23. D. Kuvshinov , P. Kurmashov, A. Bannov, M. Popov, G. Kuvshinov. Synthesis of Ni-based catalysts by hexamethylenetetramine-nitrates solution combustion method for co-production of hydrogen and nanofibrous carbon from methane, *International Journal of Hydrogen Energy*, **2019**, *44*(31), 16271-16286.

24. W. Wen , J. M. Wu, M. H. Cao. Rapid one-step synthesis and electrochemical performance of NiO/Ni with tunable macroporous architectures, *Nano Energy*, **2013**, *2*(6), 1383-1390.

25. R. Manigandan, T. Dhanasekaran, A. Dhanasekaran, K. Dhanasekaran, R. Suresh, V. Narayanan. Bifunctional hexagonal Ni/NiO nanostructures: influence of the core-shell phase on magnetism, electrochemical sensing of serotonin, and catalytic reduction of 4-nitrophenol, *Nanoscale Advances*, **2019**, *1*, 1531-1540..

26. V. D. Zhuravlev, V. G. Bamburov, L. V. Ermakova, N. I. Lobachevskaya. Synthesis of Functional Materials in Combustion Reactions, *Physics of Atomic Nuclei*, **2015**, *78*(12), 1389-1405.

27. S. J. Mammadyarova, M. B. Muradov, A. M. Maharramov, G. M. Eyvazova, Z. A. Aghamaliyev, O. O. Balayeva, I. Hasanova. Synthesis and characterization of Ni/NiO nanochains, *Materials Chemistry and Physics*, **2021**, *259*, 124171.

28. O. V. Komova, S. A. Mukha, A. M. Ozerova, O. A. Bulavchenko, A. A. Pochtar, A. V. Ishchenko, G. V. Odegova, A. P. Suknev, O. V. Netskina. New solvent-free melting-assisted preparation of energetic compound of nickel with imidazole for combustion synthesis of Ni-based materials, *Nanomaterials*, **2021**, *11*(3332), 1-20.

29. A. S. Vorokh. Scherrer formula: estimation of error in determining small nanoparticle size, *Nanosystems Physics Chemistry Mathematics*, **2018**, *9*(3), 364-369.

30. E. Mikuli, A. Migdał-Mikuli, R. Chyży, B. Grad, R. Dziembaj. Melting and thermal decomposition of $[Ni(H_2O)_6](NO_3)_2$, *Thermochimica Acta*, **2001**, *370*(1-2), 65-71.

31. I. M. Weiss, C. Muth, R. Drumm, H. O. K. Kirchner. Thermal decomposition of the amino acids glycine, cysteine, aspartic acid, asparagine, glutamic acid, glutamine, arginine and histidine, *BMC Biophysics*, **2018**, 11(2), 1-15.

32. A. Udrescu, S. Florica, M. Chivu, I. Mercioniu, E. Matei, M. Baibarac. Rhodamine B photodegradation in aqueous solutions containing nitrogen doped TiO_2 and carbon nanotubes composites, *Molecules*, **2021**, *26*, 7237.

33. A. Akkaya. The current–voltage and capacitance–voltage characterization of the Au/methylene blue/n-GaAs organic-modified Schottky diodes, *Anadolu Univ. J. of Sci. and Technology A – Appl. Sci. and Eng.*, **2018**, *19*(3), 756-767.

34. N. T. Lan, V. H. Anh, H. D. An, N. P. Hung, D. N Nhiem, B. V. Thang, P. K. Lieu, D. Q. Khieu. Synthesis of C-N-S-Tridoped TiO_2 from Vietnam ilmenite ore and its visible light-driven-photocatalytic activity for tetracyline degradation, *Journal of Nanomaterials*, **2020**, *2020*, 1-14.

35. V. T. Nguyen, V. T. Duyen, N. T. M. Binh, T. D. Manh, D. V. Duong, L. V. T. Son, T. N. Dat, L. T. Ni, H. T. H. Uyen. The synthesis of cubic $Fe_2O_3{\cdot}TiO_2$ material and its application in heterogeneous photo-Fenton degradation of dyes under visible light, *Journal of Nanoparticle Research*, **2024**, *26*(2), 1-22.

36. B. Shi, H. Yin, T. Li, J. Gong, S. Lv, Q. Nie. Synthesis of surface oxygen-deficient $BiPO_4$ nanocubes with enhanced visible light induced

photocatalytic activity, *Materials Research*, **2017**, *20*(3), 619-627.
37. T. M. Elmorsi. toward visible-light responsive photocatalysts: nano-potassium doping zinc oxide (K-ZnO) for degradation of 2-naphthol, *Physical Chemistry*, **2017**; *7*(2): 42-53.
38. A. Noua, H. Farh, R. Guemini, O. Zaoui, T. D. Ounis, H. Houadsi, H. Aounallah. Photocatalytic degradation of methylene blue by NiO thin films under solar light irradiation, *Journal of Nano Research*, **2019**, *56*, 152-157.
39. B. B. Salem, W. Ltaief, S. B. Ameur, H. Guermazi, S. Guermazi, B. Duponchel, G. Leroy. Efficient degradation of organic pollutants under solar irradiation using an n–p ZnO/NiO heterostructure, *RSC Advances*, **2025**, *15*, 13825-13837.
40. D. Lavate, V. Sawant, A. Khomane. Photodegradation of rhodamine B dye under natural sunlight using CdO, *Bulletin of Chemical Reaction Engineering & Catalysis*, **2022**, *17*(2), 466-475.
41. T. Kornprobst, J. Plank. Photodegradation of rhodamine B in presence of CaO and NiO-CaO catalysts, *International Journal of Photoenergy*, **2012**, 2012, 1-6.